Electronic properties of Au-graphene contacts

C. E. Malec and D. Davidović

Phys. Rev. B **84**, 033407 — Published 21 July 2011

DOI: 10.1103/PhysRevB.84.033407

Electronic Properties of Clean Au-Graphene Contacts

C. E. Malec and D. Davidović
School of Physics, Georgia Institute of Technology, Atlanta, GA 30332
(Dated: April 28, 2011)

The effects of Au grains on graphene conduction and doping are investigated in this report. To obtain a clean Au-graphene contact, Au grains are deposited over graphene before any chemical processing. The bulk and the effective contact resistance versus gate voltage demonstrate that Au grains cause p-doping in graphene. The Fermi level shift is in disagreement with published first principles calculations, with larger than predicted separation between the graphene and the top-most Au layer. The differential resistance versus bias voltage display anomalies at zero bias and at higher voltages, the latter likely caused by inelastic tunneling across the Au-graphene interface.

PACS numbers:

Graphene's ultrarelativistic electronic energy spectrum near the Fermi level is responsible for many interesting phenomena in electron transport. [1–4] Low carrier density and high mobility, near the charge neutrality point in graphene, suggest various possibilities for electronic devices. For example, by changing the carrier density with metal contacts, one can make p-n and p-n-p junctions. [5–10] It has been shown from first principle calculations that the electronic structure of graphene is strongly perturbed with Co, Ni, and Pd contacts, while with Al, Ag, Cu, Au, and Pt contacts, the ultrarelativistic character of the carriers in graphene remains intact. [11, 12] An intuitive explanation for the absence of hybridization between graphene and metal, in the latter case, is that the graphene K,K'-point in the reciprocal space is completely outside the free electron Fermi surface in the metal. The difference between the in-plane wavevectors reduces the coupling between the metal and the graphene wavefunctions. One consequence is a large equilibrium separation between carbon atoms in graphene and metal atoms on the surface of the metal. [11, 12] The metal contacts induce charge transfer (doping) in graphene, in response to the difference between the work functions. In this letter we investigate clean Au-graphene contacts, and find that graphene is significantly p-doped, more than expected from theory. We find that out of equilibrium electron transport through Au-graphene exhibits anomalies in differential resistance at zero voltage and at higher voltages. The latter anomalies are attributed to inelastic tunnel transitions across the Au-graphene interface.

We make graphene flakes by mechanical exfoliation from natural graphite. [13] As a substrate, we use degenerately doped Si-wafers covered with a 300nm thick thermally grown SiO_2 layer. The Si-wafer is used as a back gate. Optical contrast and Raman spectroscopy confirm single layer graphene flakes. [14] Prior measurements of the metal-graphene contact resistance show big variability; the fabrication, temperature, the metal used, and gate voltage seem to have an effect on the contact resistance. [10, 15–18] If lithography is involved between the exfoliation step and the metal deposition step, which appears to have been the case in the prior works, then polymer residue can be left in the contact, thereby changing the contact resistance. To eliminate the residue, the Au-graphene interface in our samples are made before lithography. The samples are mounted on a metal deposition stage and pumped to high vacuum (1.0×10^{-7}Torr), immediately after the exfoliation. The samples are heated in high vacuum to 250C for approximately 12 hours. After this bake-out, a Au film is deposited over the sample at ∼460°C at the rate of 1.0 Å/s, by thermal evaporation. The nominal Au film thickness is in the range 15nm-20nm. At this temperature and thickness range, Au forms isolated grains. Fig. 1A displays a sample obtained after depositing 20 nm of Au. There are three regions in the figure, corresponding to three different substrates covered by Au grains: SiO_2, a graphene flake, and a graphite flake. The morphology of Au varies among the various substrates, but individual grains are always well separated, as can be seen in Fig. 1C. The resistance over the SiO_2 is immeasurably large. The largest grains are found over the single layer graphene, where the majority of the surface is covered by grains. A more detailed picture of the grains is shown in an inset in Fig. 1A. The graphene between the grains makes channels with typical length L =35nm and width w =160nm, which is in the range previously studied by theory. [8] The grain coverage, as well as the graphene channel dimensions L and w, are affected by the amount of deposited Au, as well as the precise temperature, and substrate interactions.

Next, we make Cr/Au electric contacts to those single Au grains that overlap between the SiO_2 and the graphene substrate. Figs. 1B and C display the same graphene flake, with a variety of Cr/Au leads in contact with the overlapping grains. As highlighted in Figs. 1B and C, Cr/Au leads approach the overlapping grains from the SiO_2 side, without touching the graphene directly. We use standard electron beam lithography, with PMMA resist, CrAu deposition by metal evaporation, and lift-off. To align the CrAu leads with the grain, various grains are imaged with a scanning electron microscope and registered before lithography. After PMMA deposition and bakeout at 180C, the

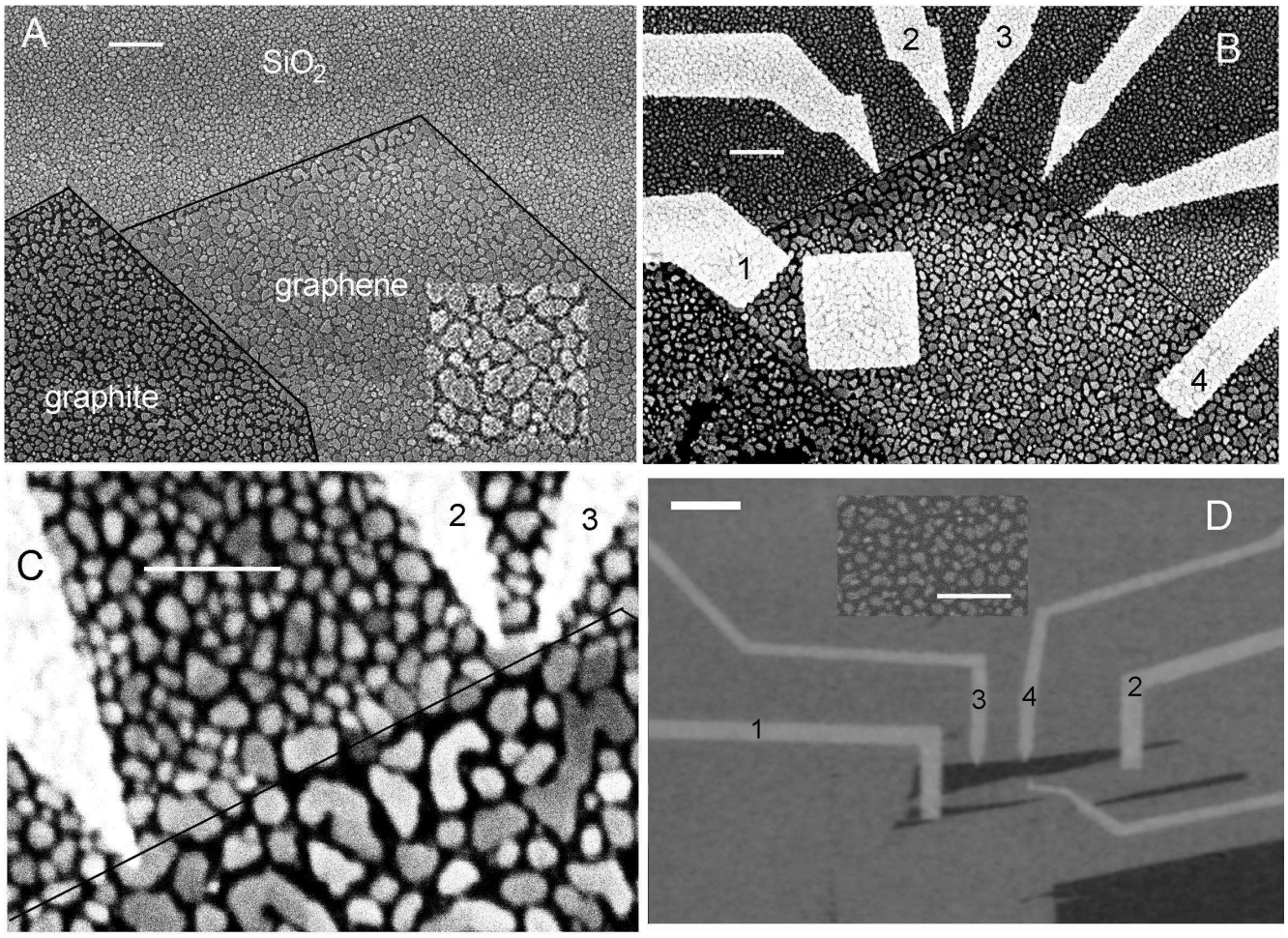

FIG. 1: A: Scanning electron micrograph of SiO_2, graphene, and graphite, covered with Au grains, in a high grain coverage sample. Inset: A square micron of grains over graphene. B: The same as in A, after Cr/Au lead deposition. C: A closer view of leads 2 and 3 from B. D: Optical image of the intermediate coverage sample. Inset: A closer view of Au grains on top of graphene from the optical image. The white bars in A-B, C and the inset of D, and the main part of D, correspond to 1μm, 0.5μm, 5μm, respectively.

leads are written with respect to the registered grains as desired, by electron beam lithography. We use grains within the 2μm×2μm square near the middle of Fig. 1B as alignment markers. We confirm that the Cr/Au leads are in good electric contact to the grains, by measuring the resistance between the leads at low temperature (kΩs). Fig. 1D displays a sample with intermediate grain coverage. We have also made control graphene samples, which have no Au grains. We have studied in detail two samples for each grain coverage, the major results presented here were reproducible among those samples. Because of the difficulty of alignment, and also because we discovered interesting features in the four probe resistance, we also fabricated devices with simple contacts without aligning to individual grains.

Fig. 2 displays four probe bulk resistance versus gate voltage at 4.2K, in the control sample (Fig. 2A); the sample with intermediate grain coverage (Fig. 2B); and the sample with high grain coverage (Fig. 2C). The resistance is measured by lock-in voltage detection, at the excitation current 100nA. As the grain coverage increases, the resistance maximum shifts to higher gate voltage, reaching $V_{g,max}$=85V in Fig. 2C, indicating p-doping in graphene in accordance with the grain coverage. Similarly, the electron-hole asymmetry in the resistance maximum increases with grain coverage. A wider resistance peak in Fig. 2B with two visible maxima and electron hole asymmetry would be qualitatively consistent with theoretical findings, [8] discrepancies may be due to the fact that in our case electrons can follow a large number of paths and the resistance curve reflects an average.

Fig. 3A shows that the bulk resistance in the high grain coverage sample, increases with the perpendicular applied

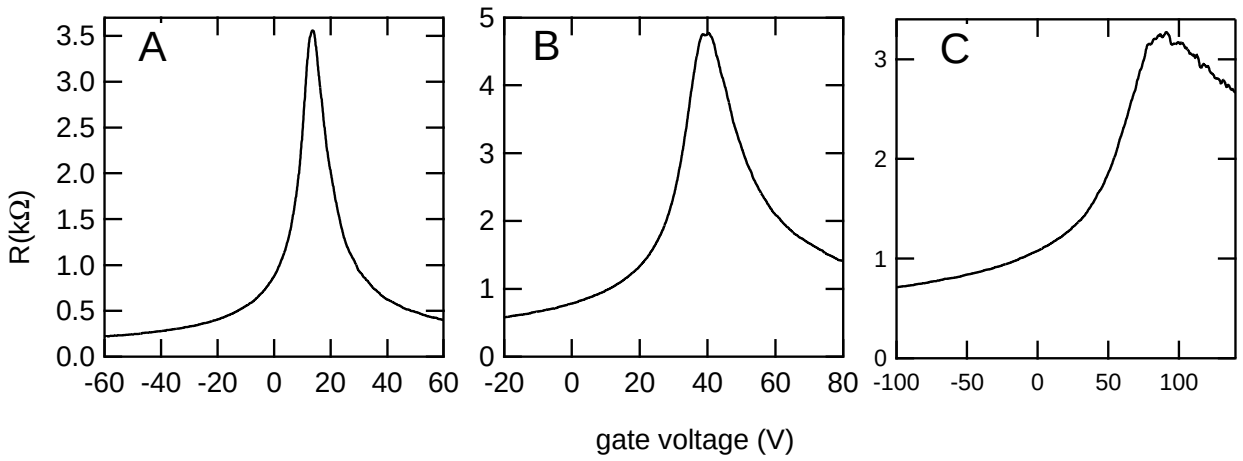

FIG. 2: A, B, C: Bulk four-probe resistance versus gate voltage, for a control sample, a sample with intermediate grain coverage, and a sample with high grain coverage, respectively. T=4.2K.

magnetic field. In the intermediate grain coverage sample, the resistance increases with magnetic field up to 8T, after which is starts to decrease with the field (not shown). Quantum Hall effect is not yet developed in that sample at 12T. In the control sample, the four probe longitudinal resistance and the Hall resistance, versus gate voltage and magnetic field, display the half-integer quantum Hall effect as expected in graphene, [1, 2] at hole mobility $5,400 cm^2/Vs$.

The electron-hole asymmetry in bulk resistance, versus grain coverage, can be explained by p-n junctions, as in Ref. [5]. Since the graphene channels in Fig. 1A are short and wide, the channels will be doped because of the proximity to the contact. [8, 9, 19] From the calculations in Refs. [9], we estimate that the charge density near the middle of the channels, at zero gate voltage, is approximately 50% of the charge density directly under the contact. At the gate voltage below the resistance maximum, both the channels and the graphene under the contact are p-doped. As the gate voltage increases, the charge neutrality will be reached in the channels first, creating p-n junctions, thereby reducing the slope in bulk resistance versus gate voltage. [5]

Next, we measure the effective contact resistance, defined as the ratio of the voltage measured between leads 3 and 4, and the current applied between leads 2 and 1. Fig. 3B displays the gate voltage dependence of the effective contact resistance, versus magnetic field. The resistance maximum is now near 120V, demonstrating that the doping is enhanced compared to the bulk. At 120V, the added electron density in graphene, induced by the gate charge, is $n = C_g V_{g,max}/|e| = 9.3 \cdot 10^{12}/cm^2$, where C_g is the capacitance to the gate per unit area, measured to be $12.4 nF/cm^2$ on a test sample from the same batch of oxidized Si-wafers. This corresponds to the p-doping in graphene with a Fermi level shift $\Delta E_F = \hbar v\sqrt{\pi n} = 0.35eV$, where we assume $v = 10^6 m/s$. First principle calculations of the Fermi level shift under a clean Au-graphene contact, under $< 111 >$ Au face, predict that $\Delta E_F = 0.19eV$ and the equilibrium separation between the carbon atoms in the graphene sheet and the Au atoms of the top-most Au layer 3.3Å. [11, 12] The calculation leads to $\Delta E_F = 0.35eV$ at the separation of $\approx 4\mathring{A}$. [11, 12]

The observed Fermi level shift is also larger than reported in previous experiments. The measurements of ΔE_F in large Ti/Au-graphene contacts, obtain $\Delta E_F = 0.25eV$ by photocurrent microscopy, [6] but those contacts involved electron-beam lithography over graphene, before the metal deposition. Photoemission spectroscopy of chemical vapor deposited graphene-metal contact with intercalation of Au monolayers displayed smaller p doping, $\Delta E_F = 0.1eV$. [20] The effects of individual Au atom adsorbates on graphene conduction have also been investigated at low temperatures. [21] Individual Au atoms lead to n-doping in graphene, but as Au-atoms bind into clusters, the Fermi level shifts back to neutrality. [21] Since the interface is clean, and the grain covers many unit cells, our results should be similar to that of bulk metal.

At zero gate voltage, the effective contact resistance is 915Ω. The contact area between the grain and graphene, estimated from the sample image, is $\approx 0.016\mu m^2$, so the effective resistivity of the contact would be $\rho = 14.6 \cdot 10^{-8}\Omega cm^2$. Alternatively, the diameter of the grain is approximately 140nm, and so the effective resistance per unit length is only $128\Omega\mu m$, comparable to the current record. [10] At -100V on the back gate, the specific contact resistance drops to $95\Omega\mu m$. The effective contact resistance measured in other similarly sized grains agrees with the above. The effective contact resistance is equal to the contact resistance only if the spread resistance from graphene under the contact and from graphene surrounding the contact is negligibly small compared to the contact resistance.

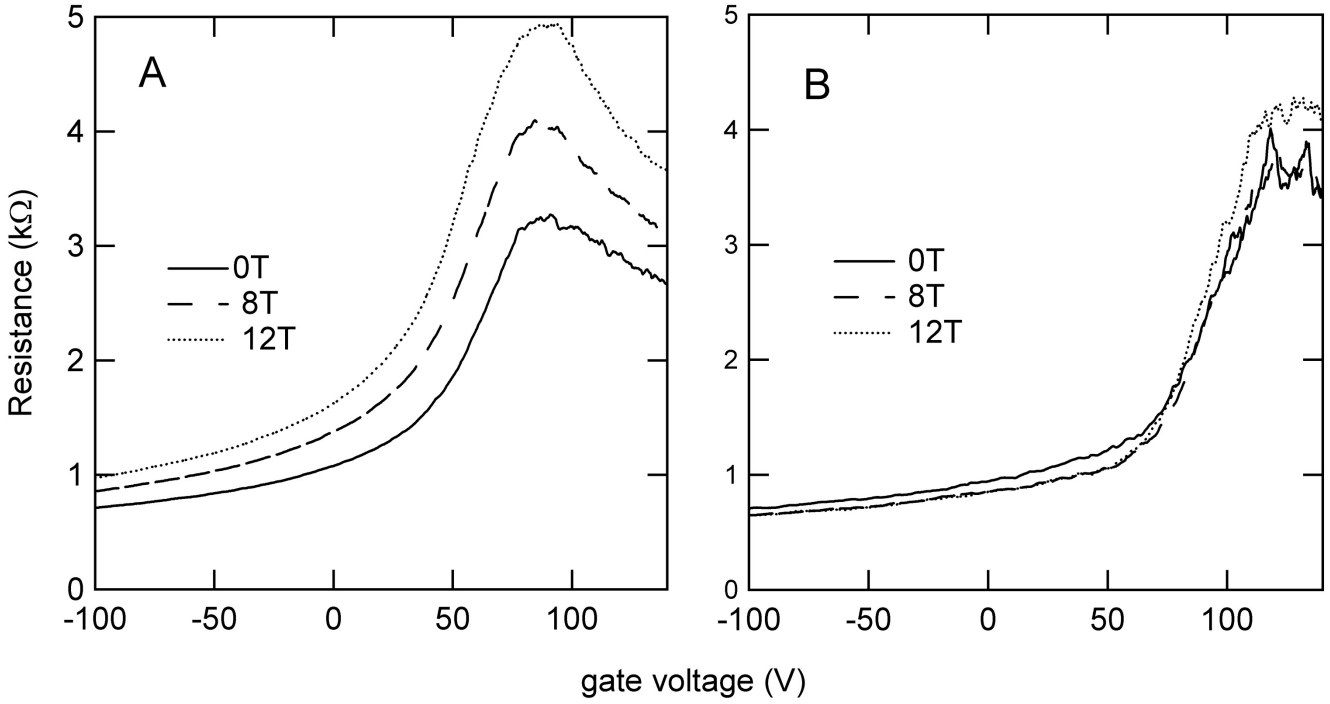

FIG. 3: A. Four probe sample resistance versus gate voltage, at 0T, 8T, and 12T. B. The effective contact resistance between the grain and graphene, versus gate voltage, at 0T, 4T, 8T, and 12T. T=4.2K.

If the spread resistance is significant, then the effective contact resistance will be larger than the contact resistance. Thus, the estimate presents an upper bound of the contact resistance. We expect that effective contact resistance is not far above the contact resistance. The contribution to the effective contact resistance from the graphene channels cannot be strong, because of the very weak magnetic field dependence of the effective contact resistance compared to the bulk (Figs. 3A and B). Also, the doping in the bulk is much weaker than in Fig. 3B.

Next, we discuss out of equilibrium electron transport. Figs. 4 A and B display bulk differential resistance versus bias voltage at 4.2K, in samples with intermediate and high grain coverage, respectively. The intermediate grain coverage sample is shown in Fig. 1D. Four-probe differential resistance dV_{34}/dI_{12} is measured and graphed versus DC bias voltage V_{12}, applied between leads 1 and 2. The gate voltage is set to approximately 15V above the Dirac point. The dominant feature in the figure is a resistance maximum near zero bias voltage, or a zero-bias anomaly (ZBA). A similar ZBA is confirmed in the control sample, although the ZBA versus magnetic field, in the control sample, exhibits oscillations between resistance maxima and minima, due to the quantum Hall effect. The discussion of the relation between the ZBA and the quantum Hall effect is outside the scope of this report.

Our Au-covered graphene samples exhibit anomalies at higher voltages as well, near 70mV and above, as indicated by arrows in Fig. 4. The anomalies are symmetric with respect to the sign of the bias voltage. The absence of anomalies at lower voltage suggests that the sample resistance is affected by some inelastic scattering process requiring an energy difference of at least 70meV. Similar fine structure has been observed in hot electron transport measurements on suspended multilayer graphene with semitransparent contact barriers. [22] It was suggested that the peaks at $V \neq 0$ arise from scattering from optical phonons. Stronger anomalies in conductance have also been observed in scanning tunneling spectroscopy in graphene, [23] and were attributed to the 67 meV out-of-plane acoustic graphene phonon modes located near the K/K' points in reciprocal space. [24] Electrons with energy less than the phonon energy, tunnel elastically between graphene and the metal. Due to the conservation of momentum, the effective barrier height of the tunneling junction is enhanced by $\hbar^2K^2/2m \approx 11eV$, so the probability of the elastic tunneling is reduced. [25–27] In inelastic tunneling, an electron at energy 67meV above the Fermi level can tunnel through the barrier with zero in plane momentum, through the emission of a K point out-of-plane phonon. [23] The barrier height for the inelastic tunneling is reduced by $11eV$ compared to that for the elastic tunneling, enhancing the probability of inelastic tunneling.

We believe that the fine structure reported here is also caused by the emission of out-of-plane acoustic graphene phonon near the K/K' points, because graphene samples without grains did not display the anomalies at higher

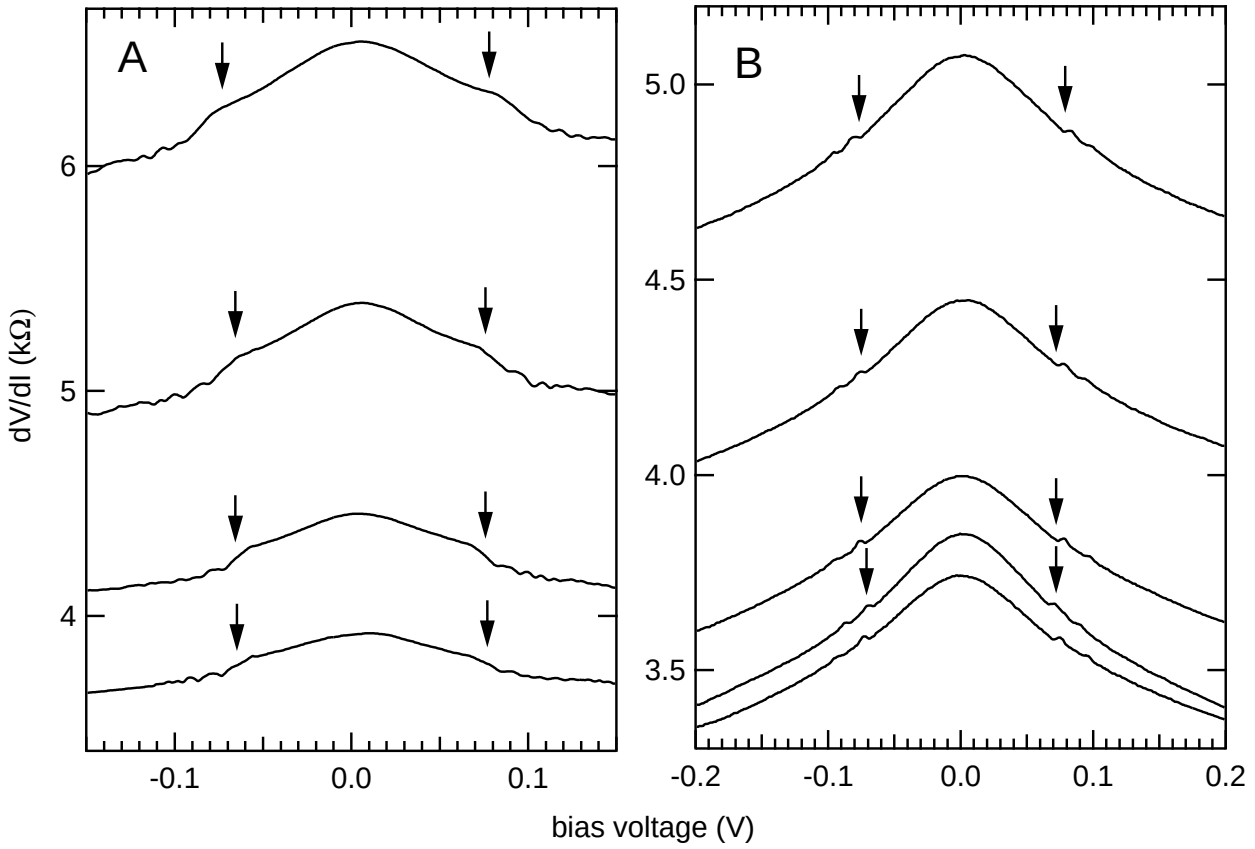

FIG. 4: A and B: Differential resistance versus bias voltage, for intermediate and dense grain coverage, respectively. Gate voltage 50V and 100V, in A and B, respectively. Both are approximately 15V above the Dirac point. In A, the applied magnetic field 0, 2T, 4T, and 6T, bottom to top. In B, the applied magnetic field 0, 2T, 4T, 6T, and 8T, bottom to top. T=4.2K.

voltages. In absence of full energy relaxation between the electronic system and the lattice, the electron distribution in graphene will have partial occupancy within an energy range $\approx eV$ about the Fermi level. Since the grains are in electric contact with graphene, the electron distribution in the grains will also be out of equilibrium. We expect that if eV is small, then the primary effect of the grains will be an enhanced elastic scattering from the grain-graphene interface and elastic tunneling across the interface, along with doping. If eV is larger than the phonon energy, than an inelastic scattering process at the graphene-Au interface will become energetically allowed. To illustrate this, consider a grain located in the middle between the source and the drain leads. An electron in graphene at energy $E_F + |eV|/2$, can make a tunneling transition into a grain level at energy $E_F - |eV|/2$ and in-plane momentum component equal to zero, while emitting the out-of-plane acoustic graphene phonon with wavevector K. Vice versa, an electron in the grain at energy $E_F + |eV|/2$ and zero in-plane momentum, could make a tunneling transition into a graphene state at energy $E_F - |eV|/2$ (near the K,K'point in the reciprocal space), while emitting the out-of-plane acoustic graphene phonon.

In conclusion, Au grains in clean contact with graphene lead to significant p-doping, with the Fermi level shift $\Delta E_F = 0.35eV$, consistent with published first principle calculations if the separation between the the graphene layer and the Au layer closest to the graphene is greater by $\approx 1\mathring{A}$ with respect to equilibrium on the $< 111 >$ face. The reason for this is not clear from the current data, though substrate interaction not included in published first principle calculations could cause such a change. Out of equilibrium electron transport in Au-covered graphene exhibits anomalies in differential resistance at high voltages, attributed to inelastic tunnel transitions across the Au-graphene interface. This work was supported by the department of energy (DE-FG02-06ER46281). We thank S. Barraza-Lopez, M. Kindermann, and M. Y. Chou for valuable discussions.

[1] K. S. Novoselov, A. K. Geim, S. V. Morozov, D. Jiang, M. I. Katsnelson, I. V. Grigorieva, S. V. Dubonos, and A. A. Firsov, Nature **438**, 197 (2005).
[2] Y. B. Zhang, Y. W. Tan, H. L. Stormer, and P. Kim, Nature **438**, 201 (2005).
[3] M. I. Katsnelson, K. S. Novoselov, and A. K. Geim, Nature Physics **2**, 620 (2006).
[4] A. F. Young and P. Kim, Nature Physics **5**, 222 (2009).
[5] B. Huard, N. Stander, J. A. Sulpizio, and D. Goldhaber-Gordon, Phys. Rev. B **78**, 121402 (2008).
[6] E. J. H. Lee, K. Balasubramanian, R. T. Weitz, M. Burghard, and K. Kern, Nature Nanotechnology **3**, 486 (2008).
[7] P. Blake, R. Yang, S. V. Morozov, F. Schedin, L. A. Ponomarenko, A. A. Zhukov, R. R. Nair, I. V. Grigorieva, K. S. Novoselov, and A. K. Geim, Solid State Communications **149**, 1068 (2009).
[8] S. Barraza-Lopez, M. Vanevic, M. Kindermann, and M. Y. Chou, Phys. Rev. Lett. **104**, 076807 (2010).
[9] P. A. Khomyakov, A. A. Starikov, G. Brocks, and P. J. Kelly, Phys. Rev. B **82**, 115437 (2010).
[10] F. Xia, V. Perebeinos, Y. ming Lin, Y. Wu, and P. Avouris, Nature Nanotechnology **6** (2011).
[11] G. Giovannetti, P. A. Khomyakov, G. Brocks, V. M. Karpan, J. van den Brink, and P. J. Kelly, Phys. Rev. Lett. **101**, 026803 (2008).
[12] P. A. Khomyakov, G. Giovannetti, P. C. Rusu, G. Brocks, J. van den Brink, and P. J. Kelly, Phys. Rev. B **79**, 195425 (2009).
[13] K. S. Novoselov, A. K. Geim, S. V. Morozov, D. Jiang, Y. Zhang, S. V. Dubonos, I. V. Grigorieva, and A. A. Firsov, Science **306**, 666 (2004).
[14] A. C. Ferrari, J. C. Meyer, V. Scardaci, C. Casiraghi, M. Lazzeri, F. Mauri, S. Piscanec, D. Jiang, K. S. Novoselov, S. Roth, et al., Phys. Rev. Lett. **97**, 187401 (2006).
[15] R. Danneau, F. Wu, M. F. Craciun, S. Russo, M. Y. Tomi, J. Salmilehto, A. F. Morpurgo, and P. J. Hakonen, Phys. Rev. Lett. **100**, 196802 (208).
[16] S. Russo, M. F. Craciun, M. Yamamoto, A. F. Morpurgo, and S. Tarucha, Physica E **42**, 677 (2010).
[17] K. Nagashio, T. Nishimura, K. Kita, and A. Toriumi, Appl. Phys. Lett. **97**, 143514 (2010).
[18] A. Venugopal, L. Colombo, and E. M. Vogel, Appl. Phys. Lett. **96**, 013512 (2010).
[19] R. Golizadeh-Mojarad and S. Datta, Phys. Rev. B **79**, 085410 (2009).
[20] A. Varykhalov, M. R. Scholz, T. K. Kim, and O. Rader, Phys. Rev. B **82**, 121101 (2010).
[21] K. M. McCreary, K. Pi, A. Swartz, W. Han, W. Bao, C. N. Lau, F. Guinea, M. I. Katsnelson, and R. K. Kawakami, Phys. Rev. B **81**, 115453 (2010).
[22] S. Lee, N. Wijesinghe, C. Diaz-Pinto, and H. B. Peng, Phys. Rev. B **82**, 045411 (2010).
[23] Y. B. Zhang, V. W. Brar, F. Wang, C. Girit, Y. Yayon, M. Panlasigui, A. Zettl, and M. F. Crommie, Nature Physics **4**, 627 (2008).
[24] M. Mohr, J. Maultzsch, E. Dobardzic, S. Reich, I. Milosevic, M. Damnjanovic, A. Bosak, M. Krisch, and C. Thomsen, Phys. Rev. B **76**, 035439 (2007).
[25] J. Tersoff and D. R. Hamann, Phys. Rev. Lett. **50**, 1998 (1983).
[26] J. Tersoff, Appl. Phys. Lett. **74**, 2122 (1999).
[27] L. Vitali, M. A. Schneider, K. Kern, L. Wirtz, and A. Rubio, Phys. Rev. B **69**, 121414 (2004).